






## Article

# Comparison of Different Approaches to the Creation of a Mathematical Model of Melt Temperature in an LD Converter

Marek Laciak <sup>\*,†</sup> , Ján Kačur <sup>†</sup> , Ján Terpák <sup>†</sup> , Milan Durdán <sup>†</sup>  and Patrik Flegner <sup>†</sup> 

Institute of Control and Informatization of Production Processes, Faculty BERG, Technical University of Košice, Némcovej 3, 042-00 Košice, Slovakia; jan.kacur@tuke.sk (J.K.); jan.terpak@tuke.sk (J.T.); milan.durdan@tuke.sk (M.D.); patrik.flegner@tuke.sk (P.F.)

\* Correspondence: marek.laciak@tuke.sk; Tel.: +421-55-602-5175

† These authors contributed equally to this work.

**Abstract:** In the steel production process in the LD converter, it is important to have information about the melt temperature. The temperature and chemical composition of the steel are important parameters in this process in terms of its completion. During the process, continuous measurement of the melt temperature and thus also information about the end of the process are missing. This paper describes three approaches to creating a mathematical model of melt temperature. The first approach is a regression model, which predicts an immeasurable melt temperature based on other directly measured process variables. The second approach to creating a mathematical model is based on the machine learning method. Simple and efficient learning algorithms characterize the machine learning methods. We used support vector regression (SVR) method and the adaptive neuro-fuzzy inference system (ANFIS) to create a mathematical model of the melt temperature. The third approach is the deterministic approach, which is based on the decomposition of the process and its heat balance. The mathematical models that were compiled based on the mentioned approaches were verified and compared to real process data.



**Citation:** Laciak, M.; Kačur, J.; Terpák, J.; Durdán, M.; Flegner, P. Comparison of Different Approaches to the Creation of a Mathematical Model of Melt Temperature in an LD Converter. *Processes* **2022**, *10*, 1378. <https://doi.org/10.3390/pr10071378>

Academic Editor: Chin-Hyung Lee

Received: 14 June 2022

Accepted: 12 July 2022

Published: 14 July 2022

**Publisher's Note:** MDPI stays neutral with regard to jurisdictional claims in published maps and institutional affiliations.



**Copyright:** © 2022 by the authors. Licensee MDPI, Basel, Switzerland. This article is an open access article distributed under the terms and conditions of the Creative Commons Attribution (CC BY) license (<https://creativecommons.org/licenses/by/4.0/>).

**Keywords:** steelmaking process; LD converter; mathematical model; temperature; machine learning methods

## 1. Introduction

Steel production is a metallurgical process of obtaining steel from iron with a lower carbon content than pig iron alloys. The steelmaking process takes place in technological equipment called a converter. The converter is part of a complex technological process of steel production. At the beginning of the process is the pig iron production in a blast furnace. Then, the pig iron is transported from the blast furnace in mixers to an out-of-furnace desulphurization plant to reduce the percentage of sulfur in the pig iron. The pig iron treated in this way continues to the steel plant, where it forms one of the important inputs for steel production in the converter. Other inputs are steel scrap and slag-forming additives to form converter slag (see Figure 1). From the point of view of the quality of produced steel, it is very important to reach the steel's required chemical composition and the steel's temperature at the end of the melt. These variables are not measured during the process (i.e., continuously) but only at the end of the melt. Mathematical methods and models are widely applicable for calculating measured process variables in various technological processes. These models are based on different approaches to their creation, e.g., Li et al. [1] proposed a new cyclone oxygen lance for the steelmaking process. The physical model and various hydrodynamic and mathematical methods were used to optimize the structure of the new oxygen lance.

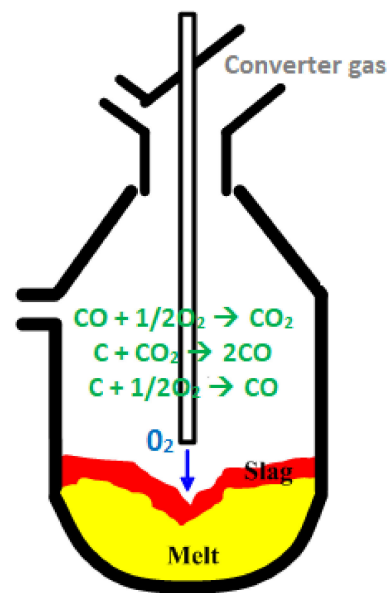


Figure 1. The LD converter.

One of the approaches for modeling steelmaking process variables is based on the thermodynamical principle. Wu et al. in [2] describe a model based on a thermodynamic equilibrium for an online prediction of the steel temperature in converters. This model is based on composition values of gas exhaust provided by a gas analyzer. The steel temperature is predicted by using this analysis and calculating the ratio of CO and CO<sub>2</sub> in the converter gas. The results showed stability in the steel temperature calculation. The authors of [3] present a mathematical model for estimating metal phases and slag composition at blow proceeds in an LD converter. It was assumed that oxidation reactions are taking place at the interface between metal phases and the slag in the emulsion. These reactions are modeled using Gibbs' free energy minimization in this interface (i.e., between metal and slag). Qualitatively good results were reached, which confirmed the need for further development of the proposed model. The modeling of the Vanadium extraction process in a basic oxygen furnace is described by Zhou and Luo [4]. These authors proposed a three-part dynamic model based on the Gibbs' free energy minimization on the slag-metal interface to study the effects of oxygen flow rate and coolant addition. The simulation results confirmed that the lack of coolant would reduce (FeO) content and elevate the molten bath temperature, and the excessive oxygen flow rate has little effect on the residual. A model for predicting flux dissolution in the oxygen steelmaking process was described by Kadrolkar et al. [5]. This model consists of the kinetic model for lime dissolution and thermodynamic models. The proposed kinetic model was considered a function of temperature and slag composition. The behavior of lime dissolution was successfully predicted using the proposed model regardless of the thermodynamic model type selected. It has been shown that for predicting the dissolution rate of lime in slag, it is necessary to consider the free lime-controlled mechanism. Oxygen converter is the subject of the research described by Jalkanen [6]. This research shows the use of a simulator, CONSIM 5, as a substitute for a static model of the oxygen converter process. The simulation results showed the necessity to create submodels for description interconnection between the sub-phenomena (i.e., post-combustion, scrap melting, etc.) and the process's main physical and technological characteristics. Furthermore, taking into account a fluid flow modeling and a mathematical model for the mass transfer of minor iron melt constituents to the oxidation environments is also necessary.

The next group of mathematical models is based on material and heat balance. A mathematical model for the improvement of the end-point control of a basic oxygen furnace (BOF) was proposed by the authors of [7]. Material and heat balance dynamic equations

are combined with the exhaust gas information in this model. The results showed that the quantity of oxygen needed for decarburization and consumed on the cavity surface of molten steel could be determined from the composition and flow rate of the gas exhausted and the quantity of oxygen and submaterials charged into BOF. Subsequently, the steel bath temperature can be calculated using the reaction theory model. Kumar et al. [8] proposed a model for predicting hot metal and slag composition at the BOF operation. This model consisted of a multi-zone kinetic model linked with a dynamic slag generation model. The three reaction zones, i.e., slag-bulk metal zone, jet impact zone, and slag-metal-gas emulsion zone, were considered for the overall refining kinetics calculation. The results obtained from a 200-ton top blowing converter showed good agreement between simulated values of metal and slag and measured data, and it was found that the post-combustion ratio is an essential factor in controlling FeO content in the slag. Dering et al. [9] describe a dynamical mathematical model to reach the economically optimal basic oxygen furnaces operation (i.e., BOFs). This model extends the work of Dogan et al. [10] and adds the model for slag formation, the energy balances model, the submodel for the decarburization in the emulsion zone and an algebraic equation for the calculation of the calcium oxide saturation in slag. The verification of the proposed model was realized on 71 melts in a real BOF. The end-point carbon content was predicted with a precision of  $\pm 0.03\%$  (for 80% melts), and the end-point temperature was predicted with a precision of  $\pm 30\text{ }^{\circ}\text{C}$  (for 61% melts). Understanding the influence of control variables (i.e., blown oxygen amount and lance height) is essential to control and optimize the basic oxygen steelmaking process. The modeling of this process is possible because the steel and slag composition cannot be measured continuously. Kattenbelt and Roffel [11] proposed a dynamic model for the main blow. This model is based on iron oxide and a carbon balance connected with the decarburization rate equation dependent on the lance height and the oxygen blowing rate. It was found that an increase in the decarburization rate is dependent on an increase in the iron ore addition rate, the oxygen blowing rate, and a decrease in lance height. The review analysis of the steelmaking process is described in [12]. This analysis is based on physical and mathematical modeling involving liquid–liquid mass transfer at the bottom gas injection. It has been found that the mass transfer coefficient is affected primarily by the gas flow rate, the injection method of this gas, the surfactants concentration, slag emulsification, etc. Furthermore, in [13], the authors describe a mathematical model of the converter process in the form of the material and heat balance. The proposed model considers the processes of slag formation, metal batch formation, converter gas formation, and blowing oxygen consumption. The results confirmed the use of the proposed model for the steel temperature calculation, determining the slag additives, determining the minimum volume of the blown oxygen, etc. The mathematical model for modeling carbon concentration was described in [14]. This model is based on the carbon's material balance in input (i.e., the pig iron and scrap) and output (i.e., carbon in CO and CO<sub>2</sub> concentration of converter gas) materials. The proposed model mostly showed lower carbon concentration values than the measured values. There was a difference in the range of  $\pm 0.06$  at 90.71% of melts,  $\pm 0.04$  at 82.14% of melts, and  $\pm 0.02$  at 63.57% of melts. The mathematical model based on the heat balance for the melt temperature determination was proposed in [15]. The rate of the melt temperature change was determined using rates of melting lime and scrap and the removal rate of unwanted elements. The temperature deviation up to 24 °C was reached at 61% of the melts.

Nowadays, machine learning and neural networks methods are increasingly used for the prediction process variables. Meradi et al. [16] proposed a model in the form of neural networks for steel temperature prediction in an LD converter. A conventional model was used to charge calculation. The presented neural networks model was based on 11 input process variables (i.e., Mn cast iron, weight scrap, weight limestone, wear of lining refractory, etc.) and steel temperature as the output variable. The mean absolute error reached 8 °C for neural networks and 30 °C for the conventional technique. Gu et al. [17] described a dynamic model of the carbon content prediction for the steelmaking process. A

long short-term memory (LSTM) model was used for this prediction. It has been found that the prediction accuracies were 25% in the  $(-0.005, 0.005)$  range, 54% in the  $(-0.010, 0.010)$  range, 71% in the  $(-0.015, 0.015)$  range, and 91% in the  $(-0.020, 0.020)$  range. The paper [18] describes three alternatives for hot steel temperature determination: time-series forecasting, infrared thermometry, and machine learning prediction. Machine learning technique based on multivariate adaptive regression splines (MARS) for hot metal temperature forecasting reached an accuracy close to that of IR thermometry but with much higher applicability (87% vs. 40%). Furthermore, there was achieved 100% applicability by the combination of measuring and modeling techniques at an error reduction of 7 °C. Andreiana et al. [19] optimized the steelmaking process using self-learning machine learning, a concretely Q-Learning algorithm. This algorithm was used as the core of a decision support system (i.e., DSS). The algorithm recommended the same actions as the operator 69.23% of the time and a better option within 30.76% of the remaining time. In the paper [20], the authors of the present article described methods for estimating melt temperature and carbon content during the oxygen steelmaking process by using a non-contact soft-sensing based on the support vector regression (SVR). It has been found that the selection of adequate pairs, i.e.,  $x_i$  and  $y_i$  (i.e., the observations and monitored targets), was the most serious problem in training the SVR model. A more realistic course was achieved by SVM regression with a polynomial kernel.

Mathematical models of the steelmaking process are also important from the point of view of process control and optimization. The dynamic control system that supports the control of the converter using a computer has been described by Takemura et al. [21]. For the target carbon content and steel temperature, these models were established: decarburizing rate model, temperature rising rate model, and control coolant evaluation model. The described control system is determined to control by conformance to decarburizing rate and temperature growing rate patterns. It has led to improved quality, steelmaking capacity, unit consumption rate, yield, etc. The model for the steelmaking process's end-point prediction based on identifying the relative decarburization rate without measuring the waste gas flow was described in [22].

## 2. Materials and Methods

### 2.1. Regression Model of the Melt Temperature

Regression analysis examines the functional relationship (course of dependence), according to which the dependent variable  $Y$  changes with changes of independent quantities  $x_1, x_2, \dots, x_k$ . We estimate the course of the dependence with suitable functions.

$$Y^o = f(x_1, x_2, \dots, x_k, b_1, b_2, \dots, b_p, \varepsilon), \quad (1)$$

where  $b_1, b_2, \dots, b_p$  are the parameters of the regression function and  $\varepsilon$  is the random deviation.

The task of regression analysis is to find a functional relationship according to which the dependent variable  $Y$  changes with the change of independent variables  $x_i$  (suitable regression function). At the same time, it is necessary to estimate the parameters of the regression function ( $b_1, b_2, \dots, b_p$ ). The regression approach to creating models for indirect measurement of temperature is based on measured process data, on the basis of which we can compile suitable regression models.

Estimates of the parameters of the regression function can be determined using the least-squares method, which is based on Gauss's multiple-verified principle: "The sum of the squares of the differences between the actual and theoretical values is the smallest possible".

$$F = \sum_{k=1}^n (Y_i - Y_i^o)^2 \rightarrow \text{MIN} \quad (2)$$

$$F = \sum_{k=1}^n (Y_i - f(x_1, x_2, \dots, x_k, b_1, b_2, \dots, b_p))^2. \quad (3)$$

By minimizing the deviation  $F$ , we get a system of Equations from which we can calculate the vector of model parameters  $b_i$  [15,23].

$$\frac{\partial F}{\partial b_i} = 0 \quad i = 1, 2, \dots, p. \quad (4)$$

In the proposal for the melt temperature regression model, we consider that the independent variables are measured variables from the converter gas analysis at the process outlet (Figure 2) and the process control variables. These variables are measured during the process and include:

- the concentration of CO in converter gas (%),
- the concentration of CO<sub>2</sub> in converter gas (%),
- the concentration of H<sub>2</sub> in converter gas (%),
- the concentration of O<sub>2</sub> in converter gas (%),
- the volume flow of converter gas (m<sup>3</sup>/hour),
- the pressure of converter gas (Pa)
- the lance height (cm),
- the volume flow of oxygen (Nm<sup>3</sup>/min).

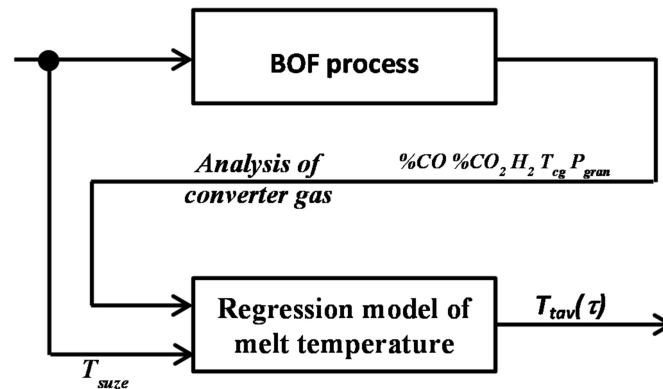


Figure 2. Scheme of the regression model.

Three variants of regression models were proposed to verify the regression model, which differs in structure. The structure of the proposed melt temperature regression models is as follows:

Model RM1:

$$T_{melt}(k+1) = b_0 + b_1.T_{cg}(k) + b_2.CO(k) + b_3.CO_2(k) + b_4.H_2(k) + b_5.T_{melt}(k); \quad (5)$$

Model RM2:

$$T_{melt}(k+1) = b_0 + b_1.T_{cg}(k) + b_2.CO(k) + b_3.CO_2(k) + b_4.H_2(k) + b_5.T_{melt}(k) + b_6.P_{gran}(k) + b_7.V_{O_2}(k); \quad (6)$$

Model RM3:

$$T_{melt}(k+1) = b_0 + b_1.T_{cg}(k) + b_2.kk_{CO}(k) + b_3.kk_{CO_2}(k) + b_4.H_2(k) + b_5.T_{melt}(k) + b_6.P_{gran}(k) + b_7.V_{O_2}(k), \quad (7)$$

where  $b_i$  are parameters of model,  $k$  is time step,  $T_{melt}$  is melt temperature (°C),  $T_{cg}$  is the temperature of converter gas (°C), CO is the concentration of CO in converter gas (%), CO<sub>2</sub> is the concentration of CO<sub>2</sub> in converter gas (%), H<sub>2</sub> is the concentration of H<sub>2</sub> in converter gas (%),  $P_{gran}$  is the pressure of converter gas on entry to the granivor (Pa),  $V_{O_2}$  is the cumulative amount of blown oxygen (m<sup>3</sup>),  $kk_{CO}$  is the cumulative concentration of CO in converter gas (%),  $kk_{CO_2}$  is cumulative concentration CO<sub>2</sub> in converter gas (%).

The regression model predicts the melt temperature during melting based on directly measured process variables. Each time step calculates the melt temperature based on the

measured variables from the previous time step. Figure 3 shows the behavior of %CO and cumulative %CO in converter gas

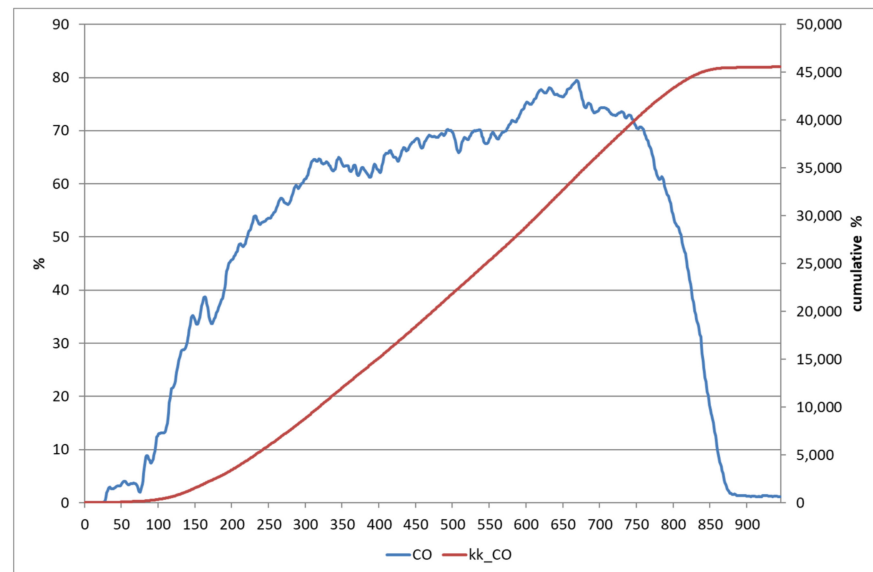


**Figure 3.** The behavior of %CO and cumulative %CO ( $kk\_CO$ ) in converter gas.

## 2.2. Deterministic Model of the Melt Temperature

Creating a complex deterministic model for the steelmaking process in the converter is a relatively demanding process, while the accuracy of the model depends mainly on the number of parameters that need to be determined. In this approach for the proposal of the melt temperature model, two models were created:

- Deterministic model with feedback;
- Simplified deterministic model without feedback.

In the deterministic model with feedback, we assume that the converter gas flow and its composition are measured, which simplifies the description of the individual sub-models. The concentrations of the individual metal impurities (% C, % Si, % Mn, % P) are calculated based on the composition of the converter gas. In the second type of deterministic model without feedback, these concentrations are calculated by approximation at known initial values (concentrations of components in pig iron) and final or required values. These concentrations form one of the inputs to the model. Figure 4 shows the schematic scheme of both deterministic models.

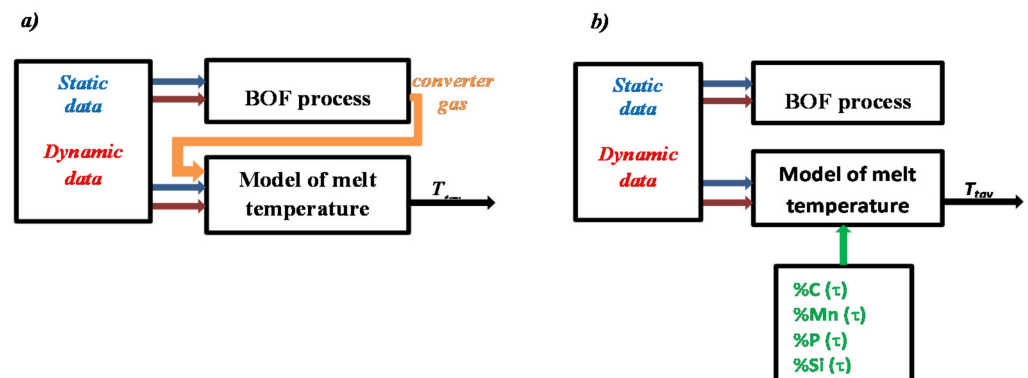


**Figure 4.** The principle scheme of deterministic models (a) model with feedback, (b) model without feedback.

### 2.2.1. The Modeled Processes of Steelmaking

The steelmaking process in the converter is a complex heterogeneous batch process with continuous oxygen input. When creating a deterministic model, we proceed from certain simplifications of selected processes, which represent:

- Scrap melting process;
- The decomposition process of slag-forming additives;
- The process of oxidation of elements C, Si, Fe, Mn, P in the melt and others.

#### Scrap melting process

The process of melting scrap is an important process in terms of heat balance, respectively, for melt temperature calculation. The description of this process is based on the heat balance and the carbon balance at the interface of scrap and molten metal, which is given by the following Equations:

$$h_{tc}(T_{me} - T_{sci}) = \frac{\lambda_{sc}}{\Delta x}(T_{sci} - T_{sc}) + \Delta H_{sc} \left( -\frac{dW_{sc}}{d\tau} \right) \quad (8)$$

$$S_{sc}\rho_{sc}k_x(C_{me} - C_{sci}) = (C_{me} - C_{sc}) \left( -\frac{dW_{sc}}{d\tau} \right), \quad (9)$$

where  $T_{me}$ ,  $T_{sc}$  are the temperature of melt and scrap ( $^{\circ}\text{C}$ ),  $T_{sci}$  is the temperature on the interference melt-scrap ( $^{\circ}\text{C}$ ),  $C_{me}$ ,  $C_{sc}$  are the concentration of carbon in melt and scrap (kg/kg),  $C_{sci}$  is the concentration of carbon on the interference melt-scrap (kg/kg),  $W_{sc}$  is the weight of scrap (kg),  $\Delta H_{sc}$  is the latent heat of scrap melting (kJ/kg),  $h_{tc}$  is heat transfer coefficient ( $\text{W}/\text{m}^2/\text{K}$ ),  $\lambda_{sc}$  is the thermal conductivity of scrap ( $\text{W}/\text{m}/\text{K}$ ),  $k_x$  is mass transfer coefficient (m/s),  $S_{sc}$  is scrap surface ( $\text{m}^2$ ),  $\rho_{sc}$  is scrap density ( $\text{kg}/\text{m}^3$ ) [7,24].

From Equations (8) and (9) it is possible to calculate the melting rate of scrap and, subsequently, from the rate of the amount of molten scrap. The molten scrap must be assigned to the melt (liquid metal), which requires a recalculation of the composition, the weight of the liquid metal, and also the calculation of the physical heat increment of the scrap according to Equation (10).

$$dQ_{fyzSr} = dM_{Sr}C_{pSr}T_{Sr}, \quad (10)$$

where  $dM_{Sr}$  is the decline of molten scrap (kg),  $C_{pSr}$  is the specific heat capacity of scrap ( $\text{J}/\text{kg}/\text{K}$ ),  $T_{Sr}$  is scrap temperature (K).

#### The decomposition process of slag-forming additives

The decomposition process of slag-forming additives is based on the decomposition of calcium carbonate.



The carbonate decomposition process only starts if the partial pressure of carbon dioxide in the gas surrounding the carbonate is less than the decomposition pressure. The following Equations give the decomposition pressure  $p_{eq}$  and the chemical reaction rate  $k_{ch}$ .

$$p_{eq} = p_{eq0}e^{-\frac{E_{eq0}}{T}} \quad (12)$$

$$k_{ch} = k_D(p_{eq} - p_{\text{CO}_2}), \quad (13)$$

where  $p_{\text{CO}_2}$  is partial pressure  $\text{CO}_2$  on the surface

$$k_D = k_{D0}e^{-\frac{E_{D0}}{T}}. \quad (14)$$

Based on Equations (12) and (14), we can write Equation (13) in the form of Equation (15). Due to porosity, the resulting velocity is mainly affected by temperature,  $\text{CO}_2$  partial

pressure, and increased total surface area. The surface magnification is modeled as the ratio of the pore surface ( $S_{por}$ ) to the geometric surface of the particle ( $S_{geom}$ ) [25].

$$k_{ch} = k_D p_{eq} - k_D p_{CO_2} \frac{S_{por}}{S_{geom}}. \quad (15)$$

With respect to the previous equations, it is possible to calculate the decomposition rate of slag-forming additives and subsequently recalculate the amount of decomposed additives from the decomposition rate of slag-forming additives. The components of the decomposed additives must be assigned to the molten metal and slag, which requires recalculation of the composition, the weight of the liquid metal and the slag, and it is also necessary to calculate the physical heat gain of the slag-forming additives  $dQ_{fyzTp}$  according to Equation (16).

$$dQ_{fyzTp} = dM_{Tp} C_{pTp} T_{Tp}, \quad (16)$$

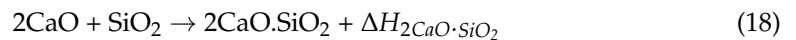
where  $dM_{Tp}$  is the decline of slag-forming additives (kg),  $C_{pTp}$  is the specific heat capacity of slag-forming additives (J/kg/K) and  $T_{Tp}$  is the temperature of slag-forming additives (K).

In addition to the physical heat, it is also necessary to consider the heat required for the decomposition of calcium carbonate Equation (17).

$$dQ_{rozVa} = dM_{Tp} x_{CO_2} \Delta H_{CaCO_3}, \quad (17)$$

where  $x_{CO_2}$  is the proportion by weight of additives attributable to  $CO_2$  from limestone (kg/kg) and  $\Delta H_{CaCO_3}$  is the thermal enthalpy of limestone decomposition (J/kg).

In the case of limestone decomposition, CaO is formed, which in the case of the available components  $SiO_2$  and  $P_2O_5$  can react in the slag according to the following Reactions.

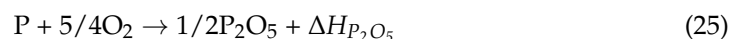
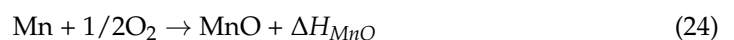
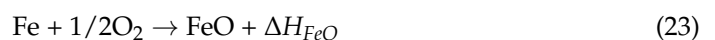


The heat that arises from the formation of slag is given by the Equation (20).

$$dQ_{tvoTr} = dM_{SiO_2} \Delta H_{2CaO \cdot SiO_2} + dM_{P_2O_5} \Delta H_{4CaO \cdot P_2O_5}. \quad (20)$$

The process of oxidation of elements

The process of oxidation of the elements C, Si, Fe, Mn, and P is described by the following chemical Reactions (21)–(25). The description of the processes is based on the assumption of the known amount and composition of blown oxygen ( $N_2$ ,  $O_2$ ) and the amount and composition ( $CO$ ,  $CO_2$ ,  $O_2$ ) of the converter gas. Flow rates ( $V_{COex}$ ,  $V_{CO_2ex}$  and  $V_{O_2ex}$ ) are calculated for the converter gas, which is determined by the product of the measured waste gas flow and the concentration of the respective component, e.g.,  $V_{COex} = V_{wg} \cdot x_{COex}$ , where  $V_{wg} = V_{wg} \cdot K_{wg}$ . The  $K_{wg}$  coefficient is evaluated at the end of each smelting as the ratio of carbon fed in pig iron and scrap to carbon in the form of  $CO$  and  $CO_2$ . This coefficient allows realizing a mass balance in the correct form.



The air intake flow  $V_{air}$  is given by Equation (26).

$$V_{air} = (V_{N_2ex} - V_{N_2bl}) / x_{N_2air}, \quad (26)$$



where  $V_{N_2ex}$  is the flow of  $N_2$  in converter gas ( $m^3/s$ ),  $V_{N_2bl}$  is the flow of  $N_2$  in blown oxygen ( $m^3/s$ ),  $x_{N_2air}$  is the concentration of  $N_2$  in the air ( $m^3/m^3$ ).

We also consider the formation of  $CO_2$  from the reaction between  $CO$  from the reaction zone and  $O_2$  from the intake air  $V_{CO_2s}$  Equation (27). The  $CO_2$  flow from the  $V_{CO_2f}$  reaction zone can be calculated by Equation (28).

$$V_{CO_2s} = 2(V_{air}x_{O_2air} - V_{O_2ex}) \quad (27)$$

$$V_{CO_2f} = V_{CO_2ex} - V_{CO_2s}, \quad (28)$$

where  $V_{O_2ex}$ ,  $V_{CO_2ex}$  is the flow  $O_2$  and  $CO_2$  in converter gas ( $m^3/s$ ).

The oxygen loss flow  $V_{O_2loss}$  is given by (29) and the effective oxygen flow  $V_{O_2eff}$  by Equation (30).

$$V_{O_2loss} = \frac{V_{CO_2f}}{2} \quad (29)$$

$$V_{O_2eff} = V_{O_2} - V_{O_2loss}. \quad (30)$$

The flow of  $CO$  from the reaction zone Equation (31) is given by the flow of  $CO$  and  $CO_2$  in the converter gas reduced by  $CO$  from the slag-forming additives, and the flow of oxygen  $V_{O_2dec}$  for decarbonization is given by Equation (32).

$$V_{COcav} = V_{COex} + V_{CO_2ex} - V_{COsub} \quad (31)$$

$$V_{O_2dec} = \frac{V_{COcav}}{2}. \quad (32)$$

The ratio of the volume of oxygen to decarbonization to the total volume of effective oxygen represents the proportion of oxygen used to oxidize the carbon Equation (33). The contribution of oxygen to the oxidation reactions of other elements is based on the rate of the respective oxidation reaction and the concentration of oxidized elements Equation (34).

$$\sigma_C = \frac{V_{O_2dec}}{V_{O_2eff}} \quad (33)$$

$$\sigma_i = \frac{k_i C_{im}}{\sum_j k_j C_{jm}} (1 - \sigma_C), \quad (34)$$

where  $i, j = Si, Fe, Mn, P$ ;  $k_i$  is the rate constant of the oxidation reaction of the  $i$ -th element,  $C_{im}$  is the concentration of the  $i$ -th element in the melt ( $kg/kg$ ).

The amount and composition of metal and slag are then calculated based on the distribution of oxygen between the individual oxidation reactions [7].

In terms of heat, it is necessary to calculate the amount of heat from exothermic oxidation reactions Equation (35) as well as the physical heat of the intake air Equation (36) and blown oxygen Equation (37).

$$Q_{exoRe} = dM_C \Delta H_{CO} + dM_{Si} \Delta H_{SiO_2} + dM_{Fe} \Delta H_{FeO} + dM_{Mn} \Delta H_{MnO} + dM_P \Delta H_{P_2O_5} \quad (35)$$

$$dQ_{fyzVz} = V_{air} C_{p,air} T_{air} \quad (36)$$

$$dQ_{fyzOx} = V_{ox} C_{p,ox} T_{ox}, \quad (37)$$

where  $V_{air}$ ,  $V_{ox}$  is the flow rate of intake air and blown oxygen ( $m^3/s$ ),  $C_{p,air}$ ,  $C_{p,ox}$  is the specific heat capacity of intake air and blown oxygen ( $J/m^3/K$ ),  $T_{air}$ ,  $T_{ox}$  is the temperature of intake air and blown oxygen (K).

### 2.2.2. The Heat Balance

The heat balance of the steelmaking process is based on the heat supplied  $Q_{pri}$ , which is given by the Equation (38).

$$Q_{pri} = Q_{surFe} + Q_{exoRe} + Q_{tvoTr} + Q_{fyzSr} + Q_{fyzOx} + Q_{fyzTp} + Q_{fyzVz}, \quad (38)$$

where  $Q_{surFe}$  is the physical and latent heat of the input pig iron (J),  $Q_{exoRe}$  is the heat from exothermic oxidation reactions of elements C, Si, Fe, Mn, P (J),  $Q_{tvoTr}$  is the heat from slag formation reactions (in creation  $2CaO.SiO_2$  and  $4CaO.P_2O_5$ ) (J),  $Q_{fyzSr}$  is the physical heat of the input steel scrap (J),  $Q_{fyzOx}$  is the physical heat of the blown oxygen (J),  $Q_{fyzTp}$  is the physical heat of the input slag-forming additives (J),  $Q_{fyzVz}$  is the physical heat of the intake air (J).

In the case of the heat consumed  $Q_{spo}$ , we consider the following items.

$$Q_{spo} = Q_{fyzMe} + Q_{fyzTr} + Q_{rozVa} + Q_{fyzKP} + Q_{fyzPr} + Q_{str}, \quad (39)$$

where  $Q_{fyzMe}$  is the physical and latent heat of the liquid metal (J),  $Q_{fyzTr}$  is the physical and latent heat of slag (J),  $Q_{rozVa}$  is the heat needed to decompose the limestone (J),  $Q_{fyzKP}$  is the physical heat of the converter gas (J),  $Q_{fyzPr}$  is physical heat of dust in converter gas (J),  $Q_{str}$  is another heat losses (J).

In the case of heat balance, i.e., equality of heat supplied and heat consumed, we can calculate the melt temperature by Equation (40).

$$T_{melt} = \frac{Q_{pri} - Q_{fyzTr} - Q_{rozVa} - Q_{fyzKP} - Q_{fyzPr} - Q_{str} - M_{me} \left( T_{me,sl} (c_{pme,s} - c_{pme,l}) + Q_{me,sl} \right)}{M_{me} c_{pme,l}}, \quad (40)$$

where  $M_{me}$  is the weight of melt (kg),  $T_{me,sl}$  is metal melting temperature (K),  $c_{pme,s}$  is the specific heat capacity of solid metal (J/kg/K),  $c_{pme,l}$  is the specific heat capacity of liquid metal (J/kg/K).

According to the previous relations, we can express all items of the heat balance and then calculate the temperature of the melt. In order to be able to implement the heat balance correctly, we need to express the heat losses  $Q_{str}$ , so we need to know the share of heat input to other unspecified losses. For this reason, three linear regression models have been proposed to calculate the heat loss coefficient ( $coef_{Qstraty}$ ). The heat loss coefficient is calculated at the beginning of the smelting based on the input parameters, which are pig iron's weight and temperature, and steel scrap's weight Equations (41)–(43).

$$coef_{Qstraty} = a_0 + a_1 T_{suze} \quad (41)$$

$$coef_{Qstraty} = a_0 + a_1 T_{suze} + a_2 m_{srot} \quad (42)$$

$$coef_{Qstraty} = a_0 + a_1 T_{suze} + a_2 m_{srot} + a_3 m_{suze}. \quad (43)$$

### 2.3. Machine Learning Model of the Melt Temperature

Another potential approach to creating a mathematical model for indirect measurement of the melt temperature in the converter is the machine learning methods.

Machine learning methods are a subset of soft computing, which deals with the recognition of so-called patterns (in terms of input-output relationship) that are observable in the examined system. Machine learning theories and algorithms fall into the artificial intelligence (AI) category. Machine learning algorithms can predict the system's future behavior based on the model created from the samples of the training set of input observations. In principle, it is a computer model based on a regression function and a large matrix of optimized  $\alpha$  support vectors (i.e., non-zero Lagrange multipliers). The model predicts on

the basis of a regression Equation (44), where it is possible to set different types of kernel functions (e.g., polynomial, Gaussian, exponential, and others).

$$f(\mathbf{x}) = \sum_{i=1}^l (\alpha_i - \alpha_i^*) k(\mathbf{x}_i, \mathbf{x}) + b. \quad (44)$$

If we consider a regression with one output variable, then the observation of the investigated object can be written as a sequence of pairs  $(\mathbf{x}_1, y_1), \dots, (\mathbf{x}_i, y_i), \dots, (\mathbf{x}_l, y_l)$ ,  $\mathbf{x}_i \in \mathbf{R}^n, y_i \in \mathbf{R}$ .

There are a number of methods and techniques in machine learning. As part of the verification of the Machine learning methodology for predicting the melt temperature, we decided to apply two methods:

- Support vector regression (SVR);
- Adaptive neuro-fuzzy inference system (ANFIS).

### 2.3.1. Support Vector Regression

Support vector regression (SVR) models are used for data prediction and classification. The basic idea is to map data to high-dimensional space through nonlinear mapping and perform linear regression in that space [26]. This mapping can be written mathematically by Equation (45).

$$f(\mathbf{x}) = (\omega \cdot \Phi(\mathbf{x})) + b \quad \text{where } \Phi(\mathbf{x}) : \mathbf{R}^n \rightarrow \mathcal{F}, \omega \in \mathcal{F} \quad (45)$$

Vector  $\mathbf{x}_i$  represents one sample of input observations  $\mathbf{x}_i = (x_{i1}, x_{i2}, \dots, x_{in})$ . In our case, it can be one line from the process data of the melt. Parameter  $b$  represents the limit value or so-called threshold. So linear regression in high-dimensional space corresponds to nonlinear regression in low-dimensional input space  $\mathbf{R}^n$ . Because  $\Phi(\mathbf{x})$  is a fixed parameter  $\omega$  we determine from the data by minimizing the amount of empirical risk  $R_{emp}[f]$  and complexity term  $\|\omega\|^2$ , which forces flatness in space  $\mathcal{F}$ . The mathematical notation of the optimization problem to be minimized has the form Equation (46).

$$R_{reg}[f] = R_{emp}[f] + \lambda \|\omega\|^2 = \sum_{i=1}^l C(f(\mathbf{x}_i) - y_i) + \lambda \|\omega\|^2, \quad (46)$$

where  $l$  is the number of samples  $(\mathbf{x}_1, \mathbf{x}_2, \dots, \mathbf{x}_l)$ ,  $C$  is the cost function,  $\lambda$  is the regularization constant. For a large set of cost functions, Equation (46) can be minimized by solving the quadratic programming problem [26]. Vector  $\omega$  can be written in terms of data points as follows:

$$\omega = \sum_{i=1}^l (\alpha_i - \alpha_i^*) \Phi(\mathbf{x}_i), \quad (47)$$

where  $\alpha_i, \alpha_i^*$  are the solution to the quadratic programming problem.

Parameters  $\alpha_i, \alpha_i^*$  have an intuitive interpretation as coating or suppression forces  $f(\mathbf{x}_i)$  to measure  $y_i$ . We can rewrite the problem as a scalar product in a low-dimensional input space [27].

$$f(\mathbf{x}) = \sum_{i=1}^l (\alpha_i - \alpha_i^*) (\Phi(\mathbf{x}_i) \cdot \Phi(\mathbf{x})) + b = \sum_{i=1}^l (\alpha_i - \alpha_i^*) k(\mathbf{x}_i, \mathbf{x}) + b. \quad (48)$$

### 2.3.2. Adaptive Neuro-Fuzzy Inference System

An adaptive neuro-fuzzy inference system or adaptive network-based fuzzy inference system (ANFIS) is a kind of artificial neural network that is based on the Takagi–Sugeno fuzzy inference system. The technique was developed in the early 1990s [28,29]. Since it integrates both neural networks and fuzzy logic principles, it has the potential to capture the benefits of both in a single framework. Its inference system corresponds to a set of fuzzy IF–THEN rules that have the learning capability to approximate nonlinear functions [30]. Hence, ANFIS is considered to be a universal estimator. For using the ANFIS in a more efficient and optimal way, one can use the best parameters obtained by a genetic algorithm [31]. It has uses in intelligent situational aware energy management systems [32].

It is possible to identify two parts in the network structure, namely the premise and consequence parts. In more detail, the architecture is composed of five layers (Figure 5) [33]. The first layer takes the input values and determines the membership functions belonging to them. It is commonly called the fuzzification layer. The membership degrees of each function are computed by using the premise parameter set, namely  $\{a,b,c\}$ . The second layer is responsible for generating the firing strengths for the rules. Due to its task, the second layer is denoted as “rule layer”. The role of the third layer is to normalize the computed firing strengths, by dividing each value by the total firing strength. The fourth layer takes as input the normalized values and the consequence parameter set  $\{p,q,r\}$ . The values returned by this layer are the defuzzification ones, and those values are passed to the last layer to return the final output [34].

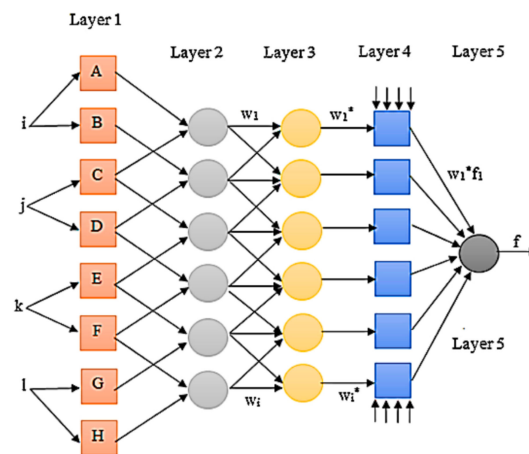


Figure 5. Adaptive neuro-fuzzy inference system (ANFIS) [33].

The first layer of an ANFIS network describes the difference to a vanilla neural network. In general, neural networks operate with a data preprocessing step, in which the features are converted into normalized values between 0 and 1. An ANFIS neural network doesn't need a sigmoid function but does the preprocessing step by converting numeric values into fuzzy ones [35].

Here is an example: suppose the network gets as input the distance between two points in the 2nd space. The distance is measured in pixels, and it can have values from 0 up to 500 pixels. Converting the numerical values into fuzzy numbers is performed with the membership function, which consists of semantic descriptions like near, middle, and far. Each possible linguistic value is given by an individual neuron. If the distance is located within the category “near”, the neuron “near” fires with a value from 0 until 1, if the distance is located within the category “near”. While the neuron “middle” fires, if the distance is in that category. The input value “distance in pixels” is split into three different neurons for near, middle, and far.

### 3. Results

The proposed models for indirect measurement of the melt temperature in the converter were verified on the basis of data from real melts (process). The results of the models are presented in terms of absolute Equation (49) and relative deviation Equation (50).

$$\Delta T_{abs} = abs\left(T^{mod}(\tau_{end}) - T^{meas}(\tau_{end})\right) \quad (49)$$

$$\Delta T_{rel} = \frac{abs\left(T^{mod}(\tau_{end}) - T^{meas}(\tau_{end})\right)}{T^{meas}(\tau_{end})} \cdot 100, \quad (50)$$

where  $T^{mod}(\tau_{end})$  is the model melt temperature  $T^{meas}(\tau_{end})$  is measured melt temperature at the end of melting.

### 3.1. Results of the Regression Model

Within the regression approach, three regression Models (5)–(7) were proposed, the results of which are shown in Table 1. The parameters of model  $b_i$  were calculated from data from other melts and were verified on a sample of data from 10 melts. In the first row of the table melt temperature ( $T^{meas}$ ) is measured at the end of the process for each melt. The next rows of the table show the model temperature for each model (RM1–RM3) and the models' calculated absolute and relative deviation.

**Table 1.** The results of the three regression models.

No. Melt	1	2	3	4	5	6	7	8	9	10
$T^{meas}$ (°C)	1655	1648	1702	1647	1656	1642	1657	1668	1665	1688
RM1 $T^{mod}$ (°C)	1651	1662	1713	1681	1688	1646	1681	1732	1680	1723
$\Delta T_{abs}$ (°C)	4.0	14.4	11.2	33.6	31.9	3.8	24.3	64.0	15.2	35.2
$\Delta T_{rel}$ (%)	0.24	0.87	0.66	2.04	1.93	0.23	1.47	3.84	0.91	2.08
RM2 $T^{mod}$ (°C)	1646	1671	1709	1648	1659	1632	1652	1688	1689	1706
$\Delta T_{abs}$ (°C)	9.3	22.7	6.6	1.1	3.1	9.9	4.5	19.9	23.8	18.0
$\Delta T_{rel}$ (%)	0.56	1.38	0.39	0.07	0.19	0.60	0.27	1.19	1.43	1.07
RM3 $T^{mod}$ (°C)	1646	1671	1709	1650	1661	1632	1653	1689	1688	1706
$\Delta T_{abs}$ (°C)	9.2	22.5	7.0	3.0	4.6	9.8	3.6	20.6	23.3	17.9
$\Delta T_{rel}$ (%)	0.55	1.37	0.41	0.18	0.28	0.60	0.22	1.23	1.40	1.06

The worst results were achieved with model RM1. The absolute temperature deviation was in the range of 3–64 °C. Models RM2 and RM3 achieved comparable results. The absolute temperature deviation was in the range of 1–24 °C. A graphical representation of the absolute deviation for all regression models is shown in Figure 6.

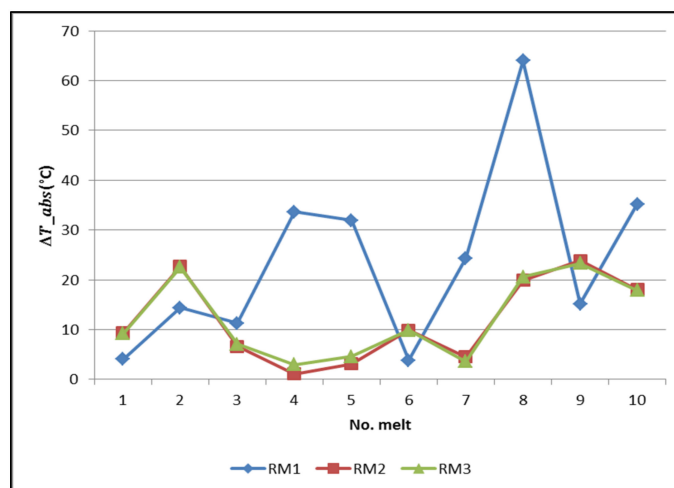


**Figure 6.** Absolute deviation of temperature for regression models.

### 3.2. Results of the Deterministic Model

The model created by the deterministic approach was verified for two variants. The first variant is a deterministic model with feedback and the second is a deterministic model without feedback. The heat losses ( $Q_{str}$ ) within the heat balance of these models were calculated using three regression Models (41)–(43).

Thus, both variants of the models were verified for the heat loss coefficient calculated according to the three models. The designation of individual model variants is as follows:

- DM1\_1—deterministic model with feedback, heat loss coefficient according to the model Equation (41).
- DM1\_2—deterministic model with feedback, heat loss coefficient according to the model Equation (42).
- DM1\_3—deterministic model with feedback, heat loss coefficient according to the model Equation (43).
- DM2\_1—deterministic model without feedback, heat loss coefficient according to the model Equation (41).
- DM2\_1—deterministic model without feedback, heat loss coefficient according to the model Equation (42).
- DM2\_1—deterministic model without feedback, heat loss coefficient according to the model Equation (43).

The results of the deterministic model with feedback are shown in Table 2, in the form of absolute and relative deviation. The results of this model are very similar for all variants of the model for calculating the heat loss coefficient. The largest absolute deviation was achieved for melt no. 4, approximately 75 °C. From the overall point of view, the best results were achieved by the DM1\_3 model, which has an average absolute deviation of about 21 °C. Figure 7 shows the average absolute deviations for the three variants of the heat loss coefficient model.

**Table 2.** The results of the deterministic model with feedback.

No. Melt	1	2	3	4	5	6	7	8	9	10
$T^{\text{meas}}$ (°C)	1655	1648	1702	1647	1656	1642	1657	1668	1665	1688
DM1_1 $T^{\text{mod}}$ (°C)	1656	1669	1694	1722	1674	1622	1642	1661	1631	1659
$\Delta T_{\text{abs}}$ (°C)	0.6	20.8	8.2	75.4	17.6	19.9	14.9	7.0	33.8	29.4
$\Delta T_{\text{rel}}$ (%)	0.04	1.26	0.48	4.58	1.06	1.21	0.90	0.42	2.03	1.74
DM1_2 $T^{\text{mod}}$ (°C)	1653	1668	1684	1723	1674	1624	1644	1664	1633	1656
$\Delta T_{\text{abs}}$ (°C)	1.9	19.8	18.3	75.9	17.7	18.4	13.3	4.3	32.4	31.7
$\Delta T_{\text{rel}}$ (%)	0.11	1.20	1.08	4.61	1.07	1.12	0.80	0.26	1.95	1.88
DM1_3 $T^{\text{mod}}$ (°C)	1641	1657	1700	1721	1670	1630	1649	1665	1636	1659
$\Delta T_{\text{abs}}$ (°C)	14.0	8.7	2.3	74.1	13.8	11.9	7.6	3.1	28.7	29.0
$\Delta T_{\text{rel}}$ (%)	0.85	0.53	0.14	4.50	0.84	0.72	0.46	0.18	1.72	1.72

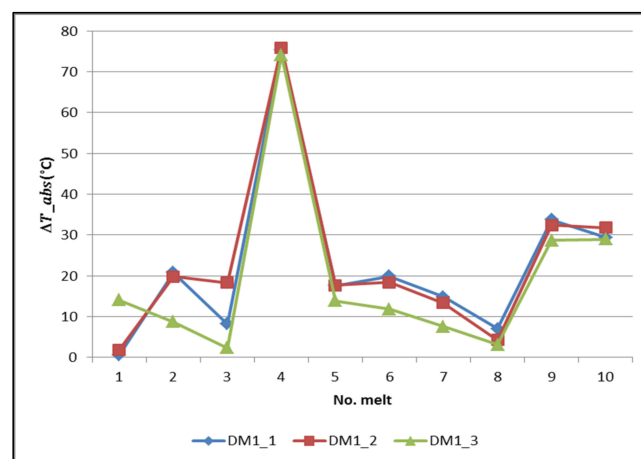


**Figure 7.** Absolute deviation of temperature for deterministic model with feedback.

The results of the deterministic model with feedback are shown in Table 3. The largest absolute deviation for this model (66 °C) was achieved for melt no. 3, a variant of model DM2\_1. The deviations achieved in the variants of the DM2\_2 and DM2\_3 models are very similar. The maximum of absolute deviation is 36 °C, which is half as much as in the DM2\_1 variant. The graphical course of absolute deviations of individual variants of the model is shown in Figure 8.

**Table 3.** The results of the deterministic model without feedback.

No. Melt	1	2	3	4	5	6	7	8	9	10
$T^{\text{meas}}$ (°C)	1655	1648	1702	1647	1656	1642	1657	1668	1665	1688
DM2_1 $T^{\text{mod}}$ (°C)	1654	1658	1768	1669	1633	1616	1619	1642	1625	1687
$\Delta T_{\text{abs}}$ (°C)	0.9	10.2	66.0	22.3	23.2	25.8	37.6	25.9	40.4	1.2
$\Delta T_{\text{rel}}$ (%)	0.06	0.62	3.88	1.35	1.40	1.57	2.27	1.55	2.42	0.07
DM2_2 $T^{\text{mod}}$ (°C)	1638	1649	1718	1660	1621	1621	1621	1644	1631	1673
$\Delta T_{\text{abs}}$ (°C)	17.0	1.2	16.2	13.4	34.7	21.3	36.0	24.1	34.5	14.8
$\Delta T_{\text{rel}}$ (%)	1.03	0.07	0.95	0.81	2.10	1.30	2.17	1.44	2.07	0.88
DM2_3 $T^{\text{mod}}$ (°C)	1639	1651	1717	1659	1621	1621	1621	1644	1631	1674
$\Delta T_{\text{abs}}$ (°C)	15.6	2.5	15.4	12.5	34.6	21.5	36.3	24.4	34.2	14.4
$\Delta T_{\text{rel}}$ (%)	0.94	0.15	0.90	0.76	2.09	1.31	2.19	1.46	2.06	0.86

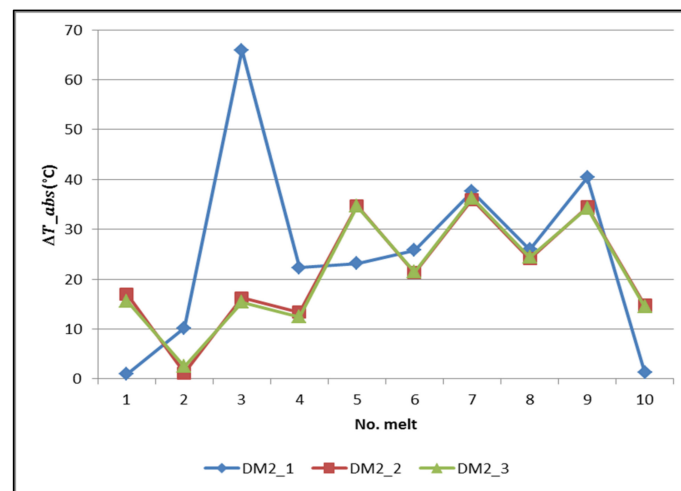


**Figure 8.** Absolute deviation of temperature for deterministic model without feedback.

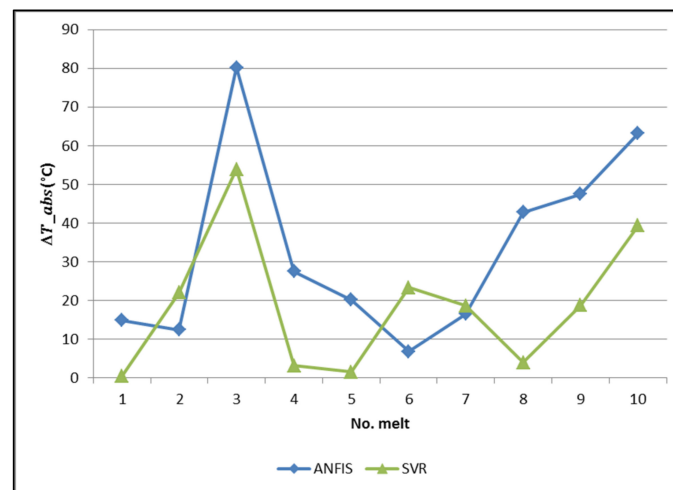
### 3.3. Results of the Machine Learning Model

As part of the machine learning approach for predicting the melt temperature, we verified two models based on the support vector regression methodology and the adaptive neuro-fuzzy inference system. The results of both models are shown in Table 4. The largest absolute deviation in both models was achieved for melt no. 3. For the SVR model it was 54 °C and for ANFIS it was 80 °C. The SVR model, which had an average absolute deviation of 18.5 °C, achieved better results. The graphical course of absolute deviations of SVR and ANFIS models is shown in the Figure 9.

Table 5 shows the results of all models and their variants in terms of average absolute and relative deviation. The best results were obtained by the regression model (RM2 and RM3), in which the value of the average absolute deviation is about 12 °C. Of the models based on the deterministic approach, it was the DM1\_3 model, whose average relative deviation is 19.3 °C. When comparing machine learning models, the SVR model achieved better results at the level of the best deterministic model.

**Table 4.** The results of the machine learning models.

No. Melt	1	2	3	4	5	6	7	8	9	10
$T^{\text{meas}} (^{\circ}\text{C})$	1655	1648	1702	1647	1656	1642	1657	1668	1665	1688
ANFIS $T^{\text{mod}} (^{\circ}\text{C})$	1640	1635	1621	1619	1635	1635	1640	1625	1617	1624
$\Delta T_{\text{abs}} (^{\circ}\text{C})$	14.8	12.4	80.2	27.5	20.2	6.8	16.5	42.7	47.5	63.2
$\Delta T_{\text{rel}} (\%)$	0.89	0.75	4.71	1.67	1.22	0.41	0.99	2.56	2.85	3.74
SVR $T^{\text{mod}} (^{\circ}\text{C})$	1655	1669	1648	1650	1657	1665	1675	1671	1646	1648
$\Delta T_{\text{abs}} (^{\circ}\text{C})$	0.4	21.9	53.9	3.1	1.5	23.3	18.6	3.9	18.7	39.3
$\Delta T_{\text{rel}} (\%)$	0.02	1.33	3.17	0.19	0.09	1.42	1.12	0.24	1.12	2.33

**Figure 9.** Absolute deviation of temperature for machine learning model.**Table 5.** Average absolute and relative deviation of models.

Model	Average Absolute Deviation ( $^{\circ}\text{C}$ )	Average Relative Deviation (%)
RM1	23.8	1.43
RM2	11.9	0.71
RM3	12.2	0.73
DM1_1	22.7	1.37
DM1_2	23.4	1.41
DM1_3	19.3	1.17
DM2_1	25.4	1.52
DM2_2	21.3	1.28
DM2_3	21.1	1.27
ANFIS	33.2	1.98
SVR	18.5	1.10

#### 4. Conclusions

The paper describes three different approaches for predicting melt temperature in the steelmaking process, i.e., regression, deterministic and machine learning approaches. Several variants of mathematical models were verified in individual approaches. Within the regression approach, three models were proposed, which differed in structure and number of independent variables. In the deterministic approach, two models were created and verified, which differ in the methodology of determining the content of impurities in the melt (i.e., % C, % Mn, % P, % Si). The heat losses in the heat balance in these two models used the support of the heat loss coefficient. In the case of the machine learning approach, two models were implemented, i.e., support vector regression (SVR) and adaptive neuro-



fuzzy inference system (ANFIS). All proposed models were verified on real process data by calculating the absolute and relative deviation of the end temperature.

Within the regression approach models, the lowest average absolute deviation was achieved by the RM2 model (11.9 °C) based on direct measurement of the concentration of CO, CO<sub>2</sub>, H<sub>2</sub> in the converter gas and on the cumulative amount of blown oxygen. The cumulative amount of blown oxygen positively affected the reduction of the deviation, which was also confirmed in the RM3 model.

In the deterministic approach, the lowest average absolute deviation (19.3 °C) was achieved by the feedback model DM1\_3, for which three parameters were used in the calculation of the heat loss coefficient, i.e., the temperature of pig iron, the weight of pig iron, and the weight of steel scrap. The positive effect of these parameters was also reflected in the model without feedback (model DM2\_3), for which the average absolute deviation was 21.1 °C.

In the case of the machine learning methods, the lowest average absolute deviation (18.5 °C) was achieved for the SVR model. This model was able to better approximate the standard dynamic course of the steelmaking process.

These results appear to be the most accurate model based on a regression approach. However, the disadvantage of these methods and machine learning methods are the high reliance on previous data approximation and on the process' dynamic. The deterministic approach based on mathematical–physical laws is not so dependent on the parameters/data of previous melts. Excluding the extreme value of the melting deviation no. 3, the average deviation of the DM1\_3 model decreased to 11.3 °C, which is comparable to the RM2 regression model. From the above, we can state that the quality of the input data greatly influences the calculation of the predicted melt temperature. For this reason, it would be appropriate to verify the proposed models on a larger set of melts and from the achieved results to select the model with the best accuracy or to use a combination of several models with acceptable accuracy. It is also necessary to minimize unspecified heat losses in the deterministic model ( $Q_{str}$ ). Very important for the accuracy of models is the measured input data from the process (e.g., the weight of pig iron, the temperature of pig iron, the concentration of elements in converter gas, etc.). Accurate measurement of these data can improve the accuracy of the model.

**Author Contributions:** Conceptualization, M.L.; Data curation, M.D.; Formal analysis, P.F. and J.T.; Methodology, J.K. and M.L.; Software, M.L., J.T. and J.K.; Project administration, M.L.; Resources, M.D. and P.F.; Supervision, M.D. and P.F.; Validation, M.L., J.T. and J.K.; Writing—Original draft preparation, M.L. and M.D.; Writing—review and editing M.D. and J.K.; All authors have read and agreed to the published version of the manuscript.

**Funding:** This research was funded by U.S. Steel Košice under works contract No. P-101-0030/17.

**Institutional Review Board Statement:** Not applicable.

**Informed Consent Statement:** Not applicable.

**Data Availability Statement:** No new data were created or analyzed in this study. Data sharing is not applicable to this article.

**Acknowledgments:** This work was supported by U.S. Steel Košice under works contract No. P-101-0030/17, and the Slovak Research and Development Agency under contract No. APVV-18-0526 and APVV-14-0892.

**Conflicts of Interest:** The authors declare no conflict of interest.

## References

1. Li, J.; Ma, Z.; Chen, C.; Zhang, J.; Wang, B. Behavior of Top-Blown Jet under a New Cyclone Oxygen Lance during BOF Steelmaking Process. *Processes* **2022**, *10*, 507. [[CrossRef](#)]
2. Ling, W.; Ningchuana, Y.; Xiangmi, Y.; Kaixin, X.; Yan, H. A Temperature Prediction Model of Converters Based on Gas Analysis. *Procedia Earth Planet. Sci.* **2011**, *2*, 14–19. [[CrossRef](#)]

3. Sarkar, R.; Gupta, P.; Basu, S. Dynamic Modeling of LD Converter Steelmaking: Reaction Modeling Using Gibbs' Free Energy Minimization. *Metall. Mater. Trans. B* **2015**, *46*, 961–976. [[CrossRef](#)]
4. Zhou, Z.; Luo, C. Dynamic Study on Vanadium Extraction Process in Basic Oxygen Furnace: Modeling Based on Gibbs' Free Energy Minimization. *Metals* **2022**, *12*, 612. [[CrossRef](#)]
5. Kadrolkar, A.; Andersson, N.I.; Dogan, N. A Dynamic Flux Dissolution Model for Oxygen Steelmaking. *Metall. Mater. Trans. B* **2017**, *48*, 99–112. [[CrossRef](#)]
6. Jalkanen, H. Experiences in physicochemical modelling of oxygen converter process (BOF), Sohn International Symposium Advanced Processing of Metals and materials Vol. 2—Thermo and physicochemical principles: Iron and Steel Making. *TMS Miner. Met. Mater. Soc.* **2006**, *2*, 541–554.
7. Takawa, T.; Katayama, K.; Katohgi, K.; Kuribayashi, T. Analysis of Converter Process Variables from Exhaust Gas. *Trans. ISIJ* **1988**, *28*, 59–67. [[CrossRef](#)]
8. Rout, B.K.; Brooks, G.; Rhamdhani, M.A.; Li, Z.; Schrama, F.; Sun, J. Dynamic Model of Basic Oxygen Steelmaking Process Based on Multi-zone Reaction Kinetics: Model Derivation and Validation. *Metall. Mater. Trans. B* **2018**, *2*, 537–557. [[CrossRef](#)]
9. Dering, D.; Swartz, C.; Dogan, N. Dynamic Modeling and Simulation of Basic Oxygen Furnace (BOF) Operation. *Processes* **2020**, *8*, 483. [[CrossRef](#)]
10. Dogan, N.; Brooks, G.A.; Rhamdhani, M.A. Comprehensive model of oxygen steelmaking part 1: Model development and validation. *ISIJ Int.* **2011**, *51*, 1086–1092. [[CrossRef](#)]
11. Kattenbelt, C.; Roffel, B. Dynamic Modeling of the Main Blow in Basic Oxygen Steelmaking Using Measured Step Responses. *Metall. Mater. Trans. B* **2008**, *39*, 764–769. [[CrossRef](#)]
12. Conejo, A.N. Physical and Mathematical Modelling of Mass Transfer in Ladles due to Bottom Gas Stirring: A Review. *Processes* **2020**, *8*, 750. [[CrossRef](#)]
13. Terpák, J.; Flegner, P.; Kačur, J.; Laciak, M.; Durdán, M.; Tréfa, G. Utilization of the Mathematical Model of the Converter Process for the Sensitivity Analysis. In Proceedings of the 2019 20th International Carpathian Control Conference (ICCC), Kraków-Wieliczka, Poland, 26–29 May 2019; IEEE: Danvers, MA, USA, 2019. [[CrossRef](#)]
14. Terpák, J.; Flegner, P.; Kačur, J.; Laciak, M.; Durdán, M.; Tréfa, G. The Mathematical Model for Indirect Measurement of Carbon Concentration in the Steelmaking Process and its Utilization in Process Control. In Proceedings of the 2021 22nd International Carpathian Control Conference (ICCC), Ostrava, Czech Republic, 31 May–1 June 2021; IEEE: Danvers, MA, USA, 2021. [[CrossRef](#)]
15. Laciak, M.; Kačur, J.; Flegner, P.; Terpák, J.; Durdán, M.; Tréfa, G. The Mathematical Model for Indirect Measurement of Temperature in the Steel-Making Process. In Proceedings of the 2020 21th International Carpathian Control Conference (ICCC), High Tatras, Slovakia, 27–29 October 2020; IEEE: Danvers, MA, USA, 2020; pp. 1–5. [[CrossRef](#)]
16. Meradi, H.; Bouhouche, S.; Lahreche, M. Prediction of Bath Temperature using Neural Networks. *Int. J. Math. Comput. Phys. Electr. Comput. Eng.* **2008**, *2*, 920–924.
17. Gu, M.; Xu, A.; Wang, H.; Wang, Z. Real-Time Dynamic Carbon Content Prediction Model for Second Blowing Stage in BOF Based on CBR and LSTM. *Processes* **2021**, *9*, 1987. [[CrossRef](#)]
18. Díaz, J.; Fernández, F.J. Application of Combined Developments in Processes and Models to the Determination of Hot Metal Temperature in BOF Steelmaking. *Processes* **2020**, *8*, 732. [[CrossRef](#)]
19. Andreiana, D.S.; Acevedo Galicia, L.E.; Ollila, S.; Leyva Guerrero, C.; Ojeda Roldán, Á.; Dorado Navas, F.; del Real Torres, A. Steelmaking Process Optimised through a Decision Support System Aided by Self-Learning Machine Learning. *Processes* **2022**, *10*, 434. [[CrossRef](#)]
20. Kačur, J.; Laciak, M.; Flegner, P.; Terpák, J.; Durdán, M.; Tréfa, G. Application of Support Vector Regression for Data Driven Modeling of Melt Temperature and Carbon Content in LD Converter. In Proceedings of the 2019 20th International Carpathian Control Conference (ICCC), Kraków-Wieliczka, Poland, 26–29 May 2019; IEEE: Danvers, MA, USA, 2019. [[CrossRef](#)]
21. Takemura, Y.; Saito, T.; Fukuda, S.; Kato, K. BOF Dynamic Control Using Sublance System. *Nippon. Steel Tech. Rep.* **1978**, *11*.
22. Terpák, J.; Flegner, P.; Kačur, J.; Laciak, M.; Durdán, M.; Tréfa, G. Endpoint Prediction of Basic Oxygen Furnace Steelmaking Based on Gradient of Relative Decarburization Rate. In Proceedings of the 2020 21th International Carpathian Control Conference (ICCC), Ostrava, Czech Republic, 31 May–1 June 2020; IEEE: Danvers, MA, USA, 2020; pp. 1–4. [[CrossRef](#)]
23. Skvarekova, E.; Tausova, M.; Senova, A.; Wittenberger, G.; Novakova, J. Statistical Evaluation of Quantities Measured in the Detection of Soil Air Pollution of the Environmental Burden. *Appl. Sci.* **2021**, *11*, 3294. [[CrossRef](#)]
24. Boser, B.E.; Guyon, I.M.; Vapnik, V.N. A Training Algorithm for Optimal Margin Classifiers. In Proceedings of the 5th Annual Workshop on Computational Learning Theory (COLT'92), Pittsburgh, PA, USA, 27–29 July 1992; pp. 144–152.
25. Mikulčić, H.; von Berg, E.; Vujanović, M.; Priesching, P.; Perković, L.; Tatschl, R.; Duić, N. Numerical modelling of calcination reaction mechanism for cement production. *Chem. Eng. Sci.* **2012**, *69*, 607–615. [[CrossRef](#)]
26. Smola, A.; Schölkopf, B. On a Kernel Based Method for Pattern Recognition, Regression, Approximation and Operator Inversion. *Algorithmica* **1998**, *22*, 211–231. [[CrossRef](#)]
27. Burges, C.J.C.; Schölkopf, B. Improving the Accuracy and Speed of Support Vector Machines. *NIPS* **1996**, 375–381.
28. Jang, J.S.R. Fuzzy Modeling Using Generalized neural Networks and Kalman Filter Algorithm. In Proceedings of the 9th National Conference on Artificial Intelligence (AAAI-91), Anaheim, CA, USA, 14–19 July 1991; Volume 4, pp. 762–767.
29. Jang, J.S.R. ANFIS: Adaptive-Network-Based Fuzzy Inference System. *IEEE Trans. Syst. Man Cybern.* **1993**, *23*, 665–685. [[CrossRef](#)]

30. Abraham, A. Adaptation of Fuzzy Inference System Using Neural Learning, Fuzzy Systems Engineering. In *Studies in Fuzziness and Soft Computing*; Nedjah, N., Macedo Mourelle, L., Eds.; Springer: Berlin/Heidelberg, Germany, 2005; Volume 181, pp. 53–83. [[CrossRef](#)]
31. Tahmasebi, P.; Hezarkhani, A. A hybrid neural networks-fuzzy logic-genetic algorithm for grade estimation. *Comput. Geosci.* **2012**, *42*, 18–27. [[CrossRef](#)] [[PubMed](#)]
32. Kamal, M.B.; Mendis, G.J.; Wei, J. Intelligent Soft Computing-Based Security Control for Energy Management Architecture of Hybrid Emergency Power System for More-Electric Aircrafts. *IEEE J. Sel. Top. Signal Processing* **2018**, *12*, 806–816. [[CrossRef](#)]
33. Ehteram, M.; Ghotbi, S.; Kisi, O.; Najah Ahmed, A.; Hayder, G.; Ming Fai, C.; Krishnan, M.; Abdulmohsin Afan, H.; EL-Shafie, A. Investigation on the Potential to Integrate Different Artificial Intelligence Models with Metaheuristic Algorithms for Improving River Suspended Sediment Predictions. *Appl. Sci.* **2019**, *9*, 4149. [[CrossRef](#)]
34. Karaboga, D.; Kaya, E. Adaptive network based fuzzy inference system (ANFIS) training approaches: A comprehensive survey. *Artif. Intell. Rev.* **2019**, *52*, 2263–2293. [[CrossRef](#)]
35. Jang, J.-S.R. Self-learning fuzzy controllers based on temporal backpropagation. *IEEE Trans. Neural Netw.* **1992**, *3*, 714–723. [[CrossRef](#)]